Calculation of the Micellar Structure of Polymer Surfactant on the Basis of the Density Functional Theory

Takashi Uneyama[†] and Masao Doi*[,‡]

Department of Physics, Graduate School of Science, Kyoto University, Sakyo-ku, Kyoto 606-8502, Japan and Department of Applied Physics, Graduate School of Engineering, The University of Tokyo, CREST JST, Hongo, Tokyo 113-8656, Japan

Received April 12, 2005

ABSTRACT: Amphiphilic block copolymer solutions form various micellar structures, including micelles and vesicles. We applied the density functional theory for block copolymers, which we have proposed, to amphiphilic block copolymer systems. The 3-dimensional (3D) simulation for AB diblock copolymer solutions and AB diblock copolymer/A homopolymer blends has been done, and it is shown that the spherical micelles, cylindrical micelles, and spherical vesicles are formed. It is also shown that the phase diagram for AB diblock copolymer/A homopolymer blends qualitatively agrees with the phase diagram obtained by the experiment.

1. Introduction

Block copolymers dissolved in solvent or other polymers assemble spontaneously to form various self-organized structures such as spheres, rods, and vesicles.[1] What structure is formed is a question very important in colloid science, but difficult to answer because the structure depends on many parameters such as the block ratio, the affinity between component units, the polymerization index, and the volume fraction of the block copolymers. Attempts have been made to predict the micellar structure by computer simulation. Because the process of self-organization involves many molecules and is very slow, atomistic molecular dynamics simulation cannot be used for this purpose.

Various coarse grained models have been used to study the formation of the micellar structure. Larson et al.[2−4] used a lattice model to show that amphiphilic molecules actually form micellar structures. Bernardes[5] studied the vesicle formation by the Larson-type lattice model. Yamamoto[7] demonstrated that dissipative particle dynamics (DPD)[6] can show the formation and various structural change of vesicles. A similar attempt has been done by Noguchi[8,9] et al. for small-molecule surfactant solutions. They studied formation and deformation of surfactant vesicles by Brownian dynamics (BD).

In these models, it is not straightforward to connect the coarse-grained model with the underlying atomistic model. (Some parameters can be associated with the mean field parameter. For example, the interaction parameters used in DPD can be mapped onto the Flory−Huggins χ parameter,[6,10] but this is not always successful and needs more validation.)

Another approach which takes into account molecular characteristics is the dynamic mean field theory, which is based on the self-consistent field (SCF) theory.[11−14] In this approach, it is possible to determine the model parameters from the atomistic models for certain classes of polymers.

For periodic systems, a computationally efficient and fast SCF method has been developed[15] that uses eigenfunctions. The method has been applied for AB diblock copolymer/A homopolymer blends that form micelles.[16] However, the method is not best suited to study the micelles or vesicles that do not form periodic structures.

For nonperiodic systems, the real-space SCF simulation method has been frequently used. The method is based on the real-space calculation of the path integral and needs large CPU power and memory. Although considerable development has been achieved because of the improvement of algorithms[11,12] and in models,[13] it is still computationally demanding for large systems.

Some work has been done for micellar systems using the real-space SCF simulation. For example, Fraaije et al.[17] and Lam et al.[18] have studied rather dense block copolymer solution with the mean field parameters calculated from the experimental data and shown that they form the micellar structure. Fraaije and Sevink[19] also demonstrated various intriguing self-organized structures formed in the droplet of concentrated solutions of block copolymers in equilibrium with the outer solvent phase.

While these applications of SCF have achieved successful results, the dilute micellar systems have not been studied yet except for a few works. He et al.[20] performed 2-dimensional (2D) SCF calculations for the dilute AB diblock copolymer solution (AB diblock copolymer/S solvent mixtures) and showed that the AB diblock copolymer actually forms 2D vesicles. Although this is an important achievement, the 2D simulation poses problems in the interpretation of the results. The spherical vesicles are 3-dimensional (3D) objects and cannot be handled by 2D simulation. At present, the 3D real-space SCF simulation for micellar systems costs too much CPU power and memory and is difficult to perform.

The computational cost of the dynamic mean field theory can be reduced drastically if one knows the free energy of the system as the functional of the density distribution of each component. The crucial point of this approach is the expression of the density functional. Earlier works[21,22] used heuristic arguments for the expression and were difficult to generalize. In the previous paper,[23] we have proposed a general expression

* Author to whom correspondence should be addressed. E-mail: doi@rheo.t.u-tokyo.ac.jp.
[†] Kyoto University.
[‡] The University of Tokyo.

10.1021/ma0507746 CCC: $30.25
Published on Web 05/27/2005

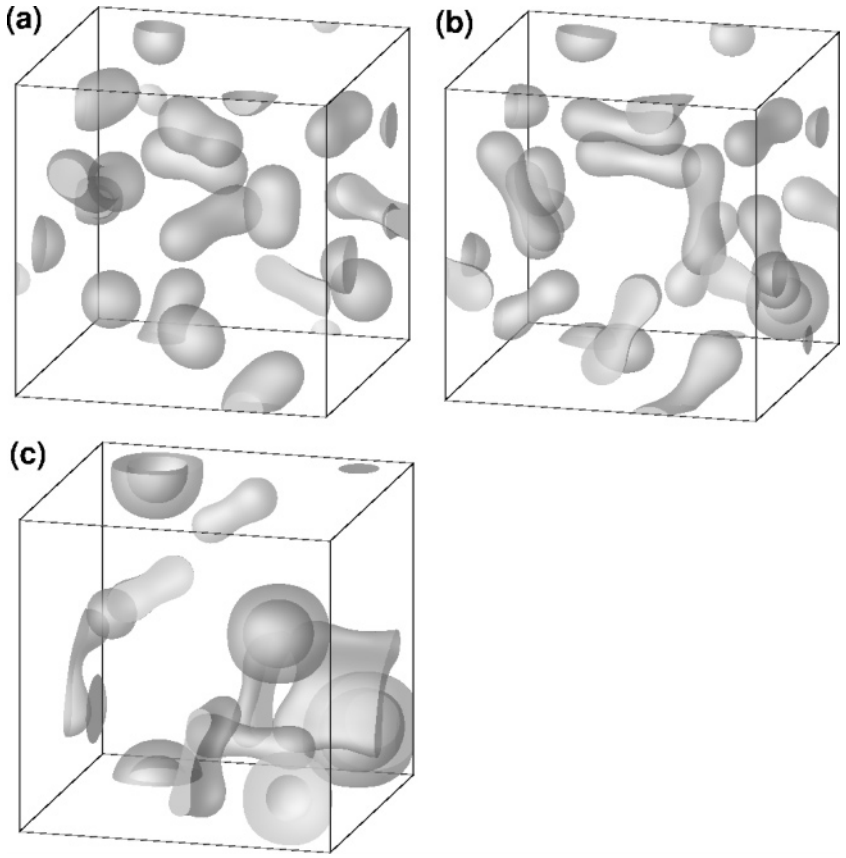

Figure 1. Micellar structures of the AB diblock copolymer solutions (AB diblock copolymer/C solvent blends) with different χ parameters. The system size is $48b \times 48b \times 48b$ ($96 \times 96 \times 96$ lattice points). Parameters are set to $N_{AB} = 20$, $N_C = 1$, $\bar{\phi}_{AB} = 0.1$, $\phi_C = 0.9$, $\chi_{AB} = 1$, $\chi_{BC} = 1.75$, $f_A = 1/3$, and $f_B = 2/3$. (a) $\chi_{AC} = 0.5$, (b) $\chi_{AC} = 0$, and (c) $\chi_{AC} = -0.175$. The gray surfaces are isodensity surfaces for $\phi_B(\boldsymbol{r}) = 0.5$.

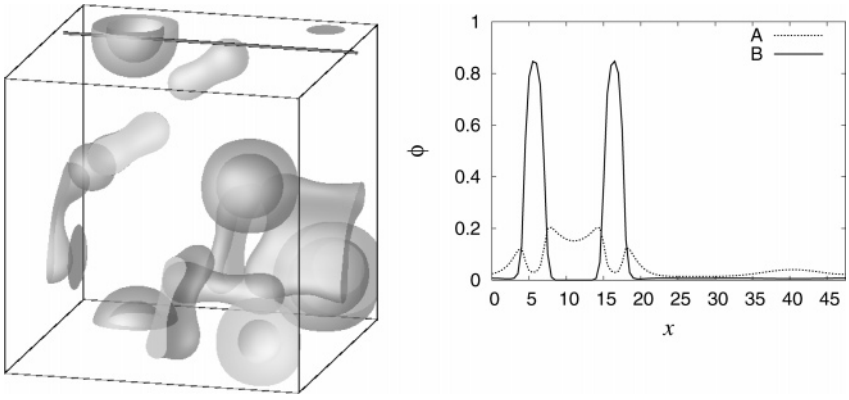

Figure 2. Density profile of an AB diblock copolymer vesicle. The parameters used are the same as Figure 1c. The 1D density profile (right) is the profile along the black line in the 3D isosurface data (left).

for the density functional that involves the same parameters appearing in the SCF theory. We have shown some preliminary results that show the formation of the self-organized structure for the mixture of block copolymers and homopolymers.

In this paper, we shall show that our free-energy functional can be applied and is effective for the study of 3D micellar systems. We shall show that micelles and vesicles are formed from the homogeneous state. (As far as we know, this is the first 3D simulation of the vesicle formation from the homogeneous state using the continuous field model.) We shall discuss the relationship between the micellar structure and the molecular parameters (volume fractions, χ parameters, the block ratio). We shall also discuss the comparison between the present simulation and experiments and the SCF simulation by He et al.[20]

2. Free Energy Functional Model

In this paper, we discuss two systems: one is the AB diblock copolymer solution (the solvent being a small molecule of C), and the other is a polymer blend, a mixture of AB diblock copolymer and A homopolymer. In both systems, the block copolymers act as the surfactant and form the self-organizing, micellar structures.

In the density functional theory, the free energy F of the system is written as a functional of the density distribution of the monomers belonging to various subchains in the system. The subchains are indexed by (p, i), where p and i refer to the polymer, and the

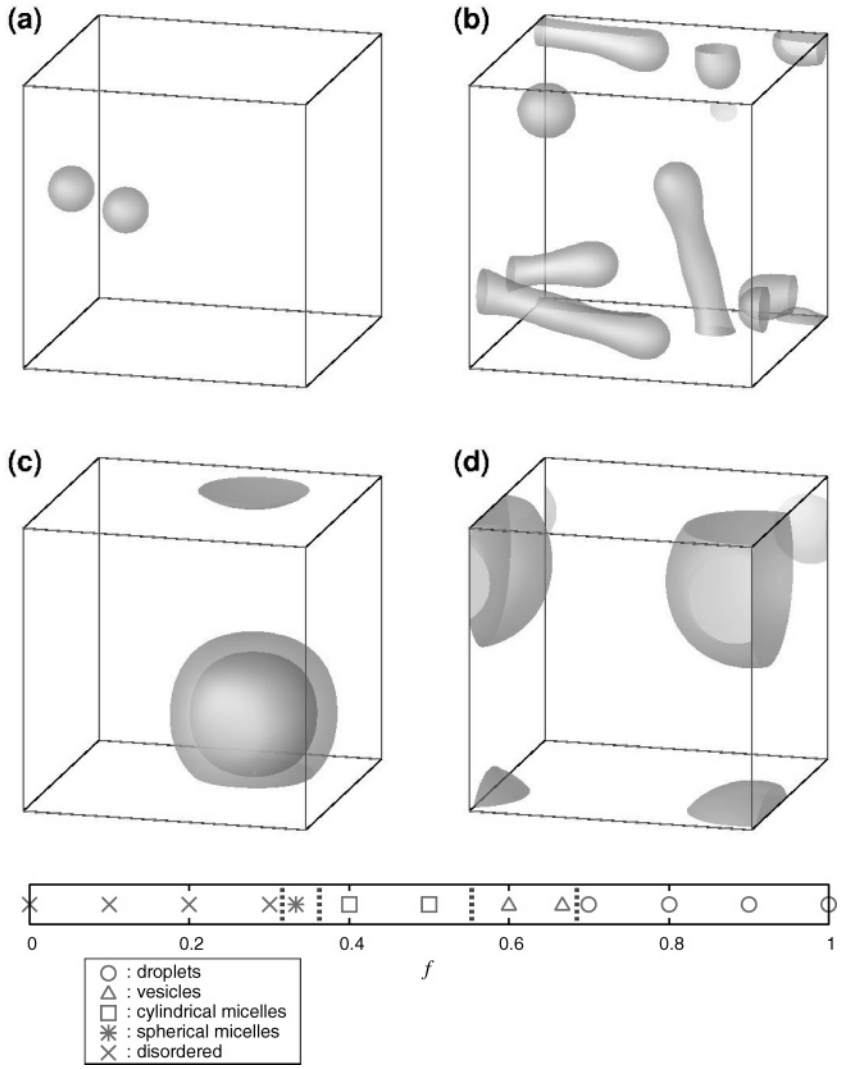

Figure 3. Phase diagram of AB diblock copolymer solutions. (a) $f_B = 1/3$, (b) $f_B = 0.5$, (c) $f_B = 0.6$, and (d) $f_B = 1$. $N_{AB} = 20$, $N_C = 1$, $\phi_{AB} = 0.1$, $\bar{\phi}_C = 0.9$, $\chi_{AB} = 1$, $\chi_{BC} = 1.75$, and $\chi_{CA} = -0.175$. System size $32b \times 32b \times 32b$, lattice points $64 \times 64 \times 64$.

subchain in the polymer. In the present problem, the system consists of three subchains (AB,A), (AB,B) and (S,S), each of which stands for the A block of the AB diblock copolymer, the B block of the AB diblock copolymer, and the matrix, which is the C solvent in the case of solution, and A homopolymer in the case of a polymer blend.

Let $\phi_{pi}(\boldsymbol{r})$ be the volume fraction of the monomers belonging to the (p, i) subchain at point $\boldsymbol{r}$. We use the following free energy functional model.[23]

$$F[\{\phi_{pi}(\boldsymbol{r})\}] = \sum_{p,ij} \int d\boldsymbol{r}d\boldsymbol{r}' 2\sqrt{f_{pi}f_{pj}}A_{p,ij}\mathscr{A}(\boldsymbol{r}-\boldsymbol{r}')\sqrt{\phi_{pi}(\boldsymbol{r})\phi_{pj}(\boldsymbol{r}')} + \sum_{pi} \int d\boldsymbol{r} f_{pi}C_{p,ii}\phi_{pi}(\boldsymbol{r}) \ln \phi_{pi}(\boldsymbol{r}) + \sum_{p,i\neq j} \int d\boldsymbol{r} 2\sqrt{f_{pi}f_{pj}}C_{p,ij}\sqrt{\phi_{pi}(\boldsymbol{r})\phi_{pj}(\boldsymbol{r})} + \sum_{pi} \int d\boldsymbol{r} \frac{b^2}{24\phi_{pi}(\boldsymbol{r})}|\nabla\phi_{pi}(\boldsymbol{r})|^2 + \sum_{pi,qj} \int d\boldsymbol{r} \frac{\chi_{pi,qj}}{2}\phi_{pi}(\boldsymbol{r})\phi_{qj}(\boldsymbol{r}) \quad (1)$$

where $\mathscr{A}(\boldsymbol{r}-\boldsymbol{r}')$ is the Green function which satisfies $-\nabla^2\mathscr{A}(\boldsymbol{r}-\boldsymbol{r}') = \delta(\boldsymbol{r}-\boldsymbol{r}')$, f_{pi} is the block ratio of the ith subchain of pth polymer, b is the effective bond length and $\chi_{pi,qj}$ is the Flory−Huggins χ parameter. $A_{p,ij}$ and $C_{p,ij}$ are determined from b, f_{pi}, the degree of polymerization N_p, and the structure of block copolymer (see ref 23 for detail).

The free energy functional eq 1 reduces to the following form for the AB diblock copolymer/S solvent blends.

$$F[\phi_A(\boldsymbol{r}), \phi_B(\boldsymbol{r}), \phi_S(\boldsymbol{r})] = \sum_{\substack{i,j \\ (=A,B)}} \int d\boldsymbol{r}d\boldsymbol{r}' 2\sqrt{f_i f_j}A_{ij}\mathscr{A}(\boldsymbol{r}-\boldsymbol{r}')\sqrt{\phi_i(\boldsymbol{r})\phi_j(\boldsymbol{r}')} + \int d\boldsymbol{r}[f_A C_{AA}\phi_A(\boldsymbol{r}) \ln \phi_A(\boldsymbol{r}) + f_B C_{BB}\phi_B(\boldsymbol{r}) \ln \phi_B(\boldsymbol{r})] + \int d\boldsymbol{r} 4\sqrt{f_A f_B}C_{AB}\sqrt{\phi_A(\boldsymbol{r})\phi_B(\boldsymbol{r})} + \int d\boldsymbol{r}\left[\frac{b^2}{24\phi_A(\boldsymbol{r})}\left|\nabla\phi_A(\boldsymbol{r})\right|^2 + \frac{b^2}{24\phi_B(\boldsymbol{r})}\left|\nabla\phi_B(\boldsymbol{r})\right|^2\right] + \int d\boldsymbol{r}\frac{1}{N_S}\phi_S(\boldsymbol{r}) \ln \phi_S(\boldsymbol{r}) + \int d\boldsymbol{r}\frac{b^2}{24\phi_S(\boldsymbol{r})}|\nabla\phi_S(\boldsymbol{r})|^2 + \sum_{\substack{i,j \\ (=A,B,S)}} \int d\boldsymbol{r}\frac{\chi_{i,j}}{2}\phi_i(\boldsymbol{r})\phi_j(\boldsymbol{r}) \quad (2)$$

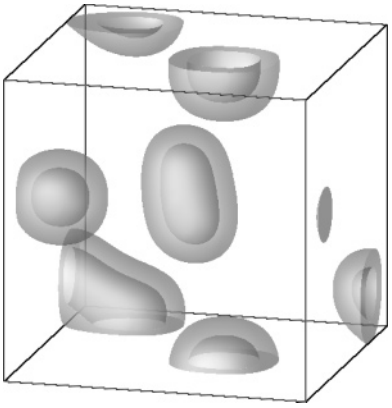

Figure 4. A result of the simulation for the AB diblock copolymer/A homopolymer blend. The system size is $64b \times 64b \times 64b$, which involves $128 \times 128 \times 128$ lattice points. The parameters of polymers are $N_{AB} = 20$, $N_A = 10$, $f_A = 1/3$, $f_B = 2/3$, and $\chi_{AB} = 1$. The volume fractions are $\bar{\phi}_{AB} = 0.1$ and $\bar{\phi}_A = 0.9$. The gray surfaces are isodensity surfaces for $\phi_B(\boldsymbol{r}) = 0.5$.

Here we dropped the index p, which specifies the polymer species, for simplicity. Thus $\phi_A(\boldsymbol{r})$, $\phi_B(\boldsymbol{r})$, and $\phi_S(\boldsymbol{r})$ stands for the density of the A component of the block copolymer, the density of the B component of the block copolymer and the density of the matrix (C solvent in the case of a polymer solution and A homopolymer in the case of a polymer blend). A_{ij} and C_{ij} for diblock copolymer (i, j = A, B) is given in Appendix A.

It is convenient to introduce the new order parameter (the ψ field) defined via the following equation:[23]

$$\psi_i(\boldsymbol{r}) \equiv \sqrt{\phi_i(\boldsymbol{r})} \tag{3}$$

With this order parameter, eq 2 is rewritten as

$$\begin{aligned} F[\psi_A(\boldsymbol{r}), \psi_B(\boldsymbol{r}), \psi_S(\boldsymbol{r})] = \\ \sum_{\substack{i,j \\ (=A,B)}} \int d\boldsymbol{r} d\boldsymbol{r}' 2\sqrt{f_i f_j} A_{ij} \mathscr{G}(\boldsymbol{r} - \boldsymbol{r}') \psi_i(\boldsymbol{r}) \psi_j(\boldsymbol{r}') + \\ \int d\boldsymbol{r} [2 f_A C_{AA} \psi_A^2(\boldsymbol{r}) \ln \psi_A(\boldsymbol{r}) + 2 f_B C_{BB} \psi_B^2(\boldsymbol{r}) \ln \psi_B(\boldsymbol{r})] + \\ \int d\boldsymbol{r} 4\sqrt{f_A f_B} C_{AB} \psi_A(\boldsymbol{r}) \psi_B(\boldsymbol{r}) + \\ \int d\boldsymbol{r} \left[\frac{b^2}{6} \left| \nabla \psi_A(\boldsymbol{r}) \right|^2 + \frac{b^2}{6} \left| \nabla \psi_B(\boldsymbol{r}) \right|^2 \right] + \\ \int d\boldsymbol{r} \frac{2}{N_S} \psi_S^2(\boldsymbol{r}) \ln \psi_S(\boldsymbol{r}) + \int d\boldsymbol{r} \frac{b^2}{6} |\nabla \psi_S(\boldsymbol{r})|^2 + \\ \sum_{\substack{i,j \\ (=A,B,S)}} \int d\boldsymbol{r} \frac{\chi_{i,j}}{2} \psi_i^2(\boldsymbol{r}) \psi_j^2(\boldsymbol{r}) \end{aligned} \tag{4}$$

3. Simulation

We performed the simulation to get the equilibrium structure of the diblock copolymer solution. To get the equilibrium structure numerically, we minimized the free-energy functional eq 4 by using the algorithm shown in this section.

3.1. Constraints. The minimization of the free energy was done under two constraints, each representing the conservation condition and the incompressible condition.

$$\int d\boldsymbol{r} \psi_i^2(\boldsymbol{r}) = V \bar{\phi}_i, \quad (i = A, B, S) \tag{5}$$

$$\sum_{i(=A,B,S)} \psi_i^2(\boldsymbol{r}) = 1 \tag{6}$$

where V is the volume of the system and $\bar{\phi}_i$ is the spatial average of $\phi_i(\boldsymbol{r})$. $\bar{\phi}_S$ is the average volume fraction of solvent and $\bar{\phi}_A$, $\bar{\phi}_B$ are given by the following equations:

$$\bar{\phi}_A = f_A \bar{\phi}_{AB} \tag{7}$$

$$\bar{\phi}_B = f_B \bar{\phi}_{AB} \tag{8}$$

where $\bar{\phi}_{AB}$ is the average volume fraction of the AB diblock copolymer. $\bar{\phi}_{AB}$ and $\bar{\phi}_S$ satisfy the following equation:

$$\bar{\phi}_{AB} + \bar{\phi}_S = 1 \tag{9}$$

Constraints eqs 5 and 6 give the following terms for the free energy functional (4).

$$\begin{aligned} F_{\text{constraints}}[\psi_A(\boldsymbol{r}), \psi_B(\boldsymbol{r}), \psi_S(\boldsymbol{r})] = \\ \sum_i \int d\boldsymbol{r} \frac{1}{2} [\lambda_i + \kappa(\boldsymbol{r})] [\psi_i^2(\boldsymbol{r}) - \bar{\phi}_i] \end{aligned} \tag{10}$$

where λ_i and $\kappa(\boldsymbol{r})$ are the Lagrangian multipliers that correspond to the conservation and incompressible conditions, respectively.

3.2. Numerical Scheme. The free energy was minimized by evolving the ψ field iteratively by using the steepest-descent method.

$$\psi_i^{(\text{new})}(\boldsymbol{r}) = \psi_i(\boldsymbol{r}) - \omega [\mu_i(\boldsymbol{r}) + \lambda_i \psi_i(\boldsymbol{r}) + \kappa(\boldsymbol{r}) \psi_i(\boldsymbol{r})] \tag{11}$$

where ω is a positive constant and $\mu_i(\boldsymbol{r})$ is the chemical potential defined as

$$\mu_i(\boldsymbol{r}) \equiv \frac{\delta F[\psi_A(\boldsymbol{r}), \psi_B(\boldsymbol{r}), \psi_S(\boldsymbol{r})]}{\delta \psi_i(\boldsymbol{r})} \tag{12}$$

By substituting eq 4 into eq 12, we get the explicit form of the chemical potential (See Appendix B for details).

We employed the time-splitting method and the ADI method[24] to update $\psi^{(\text{new})}(\boldsymbol{r})$ from $\psi(\boldsymbol{r})$ by eq 11.

$$\psi_i^{(1)}(\boldsymbol{r}) = \psi_i(\boldsymbol{r}) - \omega^{(1)} \left\{ \left[\mu_i(\boldsymbol{r}) + \frac{b^2}{3} \frac{\partial^2 \psi_i(\boldsymbol{r})}{\partial x^2} \right] - \frac{b^2}{3} \frac{\partial^2 \psi^{(1)}(\boldsymbol{r})}{\partial x^2} \right\} \tag{13}$$

$$\psi_i^{(2)}(\boldsymbol{r}) = \psi_i^{(1)}(\boldsymbol{r}) - \omega^{(1)} \left\{ \left[\mu_i^{(1)}(\boldsymbol{r}) + \frac{b^2}{3} \frac{\partial^2 \psi_i^{(1)}(\boldsymbol{r})}{\partial y^2} \right] - \frac{b^2}{3} \frac{\partial^2 \psi^{(2)}(\boldsymbol{r})}{\partial y^2} \right\} \tag{14}$$

$$\psi_i^{(3)}(\boldsymbol{r}) = \psi_i^{(2)}(\boldsymbol{r}) - \omega^{(1)} \left\{ \left[\mu_i^{(2)}(\boldsymbol{r}) + \frac{b^2}{3} \frac{\partial^2 \psi_i^{(2)}(\boldsymbol{r})}{\partial z^2} \right] - \frac{b^2}{3} \frac{\partial^2 \psi^{(3)}(\boldsymbol{r})}{\partial z^2} \right\} \tag{15}$$

$$\psi_i^{(4)}(\boldsymbol{r}) = \psi_i^{(3)}(\boldsymbol{r}) - \omega^{(2)} \kappa(\boldsymbol{r}) \psi_i^{(3)}(\boldsymbol{r}) \tag{16}$$

$$\psi_i^{(\text{new})}(\boldsymbol{r}) = \psi_i^{(4)}(\boldsymbol{r}) - \omega^{(3)} \lambda_i \psi^{(4)} \tag{17}$$

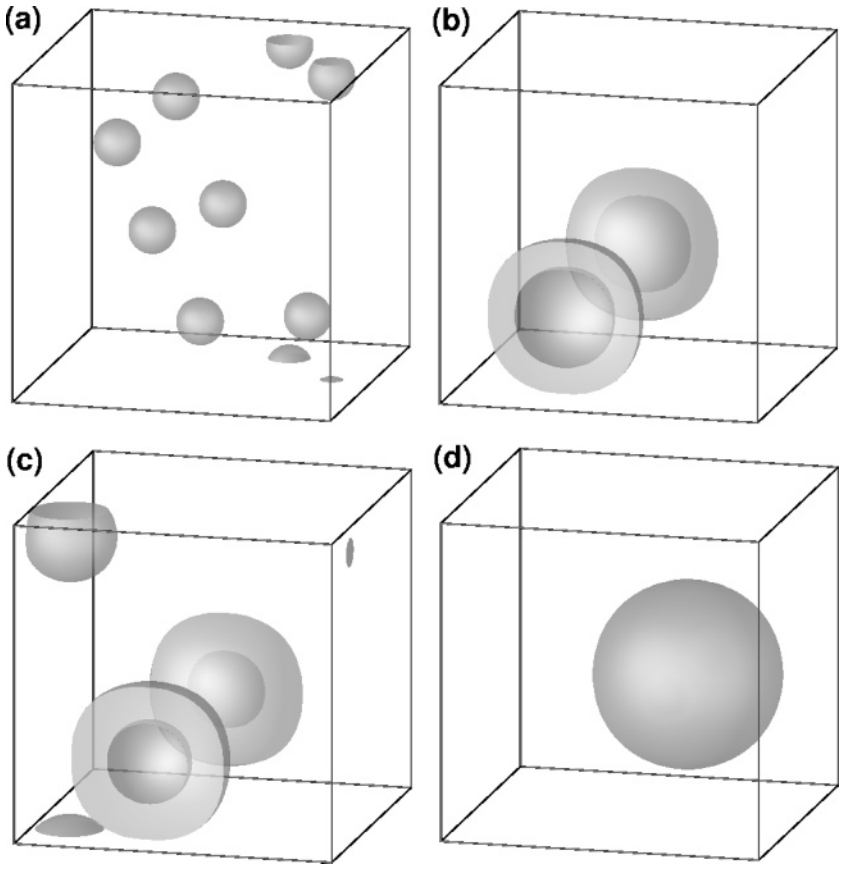

Figure 5. Results of simulations with different block ratios. The system size is $32b \times 32b \times 32b$. $N_{AB} = 20$, $N_A = 10$, $\bar{\phi}_{AB} = 0.1$, $\bar{\phi}_A = 0.9$, and $\chi_{AB} = 1$. (a) $f_B = 1/3$, (b) $f_B = 0.5$, (c) $f_B = 2/3$, and (d) $f_B = 1$. The gray surfaces are isodensity surfaces for $\phi_B(\boldsymbol{r}) = 0.5$.

where $\omega^{(n)}$ is positive constant and $\mu_i^{(n)}$ is the chemical potential calculated from $\psi_i^{(n)}(\boldsymbol{r})$. The advantage of using the ADI method is that we can choose a large value for ω compared with one used in the explicit method that we employed in our previous work.[23] The evolution with eq 17 can be regarded as rescaling of the ψ field to satisfy the conservation law (this is analogous to the wave function in quantum mechanics; we normalize the wave function to get probability density). Thus, eq 17 was modified as follows:

$$\psi_i^{(\mathrm{new})}(\boldsymbol{r}) = \sqrt{\frac{V\bar{\phi}_i}{\int \mathrm{d}\boldsymbol{r}[\psi_i^{(4)}(\boldsymbol{r})]^2}}\,\psi_i^{(4)}(\mathbf{r}) \qquad (18)$$

We also evolved $\kappa(\boldsymbol{r})$ as well.

$$\kappa^{(\mathrm{new})}(\boldsymbol{r}) = \kappa(\boldsymbol{r}) - \omega^{(4)}[\psi_i^2(\boldsymbol{r}) - \bar{\phi}_i] \qquad (19)$$

Equations 13−16, 18, and 19 were solved iteratively to get the steady-state structure. All simulations were started from the nearly homogeneous state with small Gaussian white noise, and the periodic boundary condition was used. The evolution was conducted until the ψ fields do not change anymore. This structure is not necessarily the equilibrium structure; in most cases, it is a metastable structure. As our purpose is to search various metastable structures, we did not pursue finding the real minimum of the free energy.

The numerical scheme described above produces the equilibrium (or metastable) structure efficiently. For example, we can get 3D AB diblock copolymer vesicles (lattice points: $128 \times 128 \times 128$, detail parameters are shown in the following section) starting from the homogeneous state in about 26 h on a 3.0 GHz Pentium 4 PC.

For the systems with small volume fraction of the block copolymer and/or a small χ parameter, spontaneous formation of the self-organized structure from the homogeneous state was not always successful. It is difficult to get the micellar structure by our scheme, especially for these systems. Thus, we used the following procedure.

We started the simulations from the nearly homogeneous state by using a rather large χ parameter (for example $\chi_{AB} = 1$) and/or large volume fraction (for example $\bar{\phi}_{AB} = 0.1$). This gives a state which has a large density fluctuation after several hundred iteration steps. We then switched χ_{AB} and $\bar{\phi}_{AB}$ to the target value and continued the simulation for several thousand iteration steps (about 2000 to 4000 in this work) to get the equilibrium state. As arbitrary and artificial it may look, such a procedure was needed to get the phase-separated structure. In fact, without the procedure, we could not reproduce the phase separation in the region where the χ parameter or the volume fraction are small.

4. Results

4.1. AB Diblock Copolymer Solutions (AB Diblock Copolymer/C Solvent). First we show the result of the simulation for the AB diblock copolymer solutions. We set the A monomer as solvent-philic and the B monomer as solvent-phobic (i.e. the χ parameter between the A and C monomers is small or negative, and that between the B and C monomers is large).

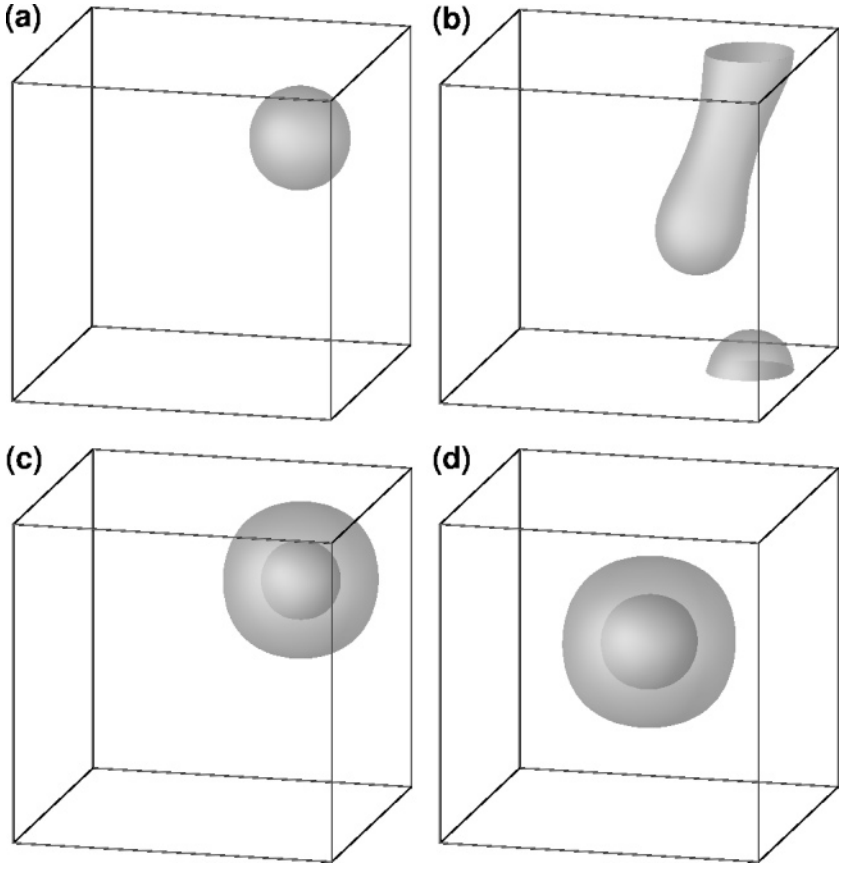

Figure 6. Results of simulations with different volume fractions. The system size is $32b \times 32b \times 32b$. $N_{AB} = 20$, $N_A = 10$, $f_A = 1/3$, $f_B = 2/3$, and $\chi_{AB} = 1$. (a) $\bar{\phi}_{AB} = 0.025$, (b) $\bar{\phi}_{AB} = 0.0525$, (c) $\bar{\phi}_{AB} = 0.075$, and (d) $\bar{\phi}_{AB} = 1$. The gray surfaces are isodensity surfaces for $\phi_B(\boldsymbol{r}) = 0.5$.

Figure 1 shows the result of the simulation. Here, the surfactant is a medium-sized block copolymer ($N_{AB} = 20$) with a short solvent-philic part ($f_A = 1/3$) and a long solvent-phobic part ($f_B = 2/3$). The other parameters are $N_C = 1$, $\bar{\phi}_{AB} = 0.1$, $\bar{\phi}_C = 0.9$, $\chi_{AB} = 1$, $\chi_{BC} = 1.75$, and χ_{AC} are taken to be 0.5 (a), 0 (b), and -0.175 (c). The system size is $48b \times 48b \times 48b$, and the number of lattice points is $96 \times 96 \times 96$.

The figure demonstrates that the density functional method gives self-organized structures, spontaneously starting from a nearly homogeneous initial state. Various micellar structures, spherical micelles, cylindrical micelles, open bilayers (not closed membrane structures), and vesicles are observed. Notice that the micellar structure is not the same; there is a distribution of micellar size as well as the micellar structure. We believe that a real micellar system will also have such distribution.

The morphological change shown in Figure 1 can be qualitatively understood as follows. As χ_{AC} decreases, the affinity between the solvent and the solvent-philic part increases. Therefore, the interfacial area between the micelles and solvent tends to increase. As a result, the micellar structure changes from spheres to cylinders and then to vesicles.

Figure 2 shows the 1-dimensional (1D) density profile of Figure 1c. It is observed that the AB diblock copolymer is strongly localized at the micellar structure (the vesicle) and the density of unimers are quite small.

To investigate the effect of the architecture of block copolymers, we fixed the parameters, except for the block ratio, and performed several simulations with different block ratio. The parameters are set to $N_{AB} = 20$, $N_C = 1$, $\bar{\phi}_{AB} = 0.1$, $\bar{\phi}_C = 0.9$, $\chi_{AB} = 1$, $\chi_{BC} = 1.75$, $\chi_{CA} = -0.175$, system size $32b \times 32b \times 32b$, lattice points $64 \times 64 \times 64$, and the simulations have been done for block ratios $f_B = 0$, 0.1, 0.2, 0.3, $1/3$, 0.4, 0.5, 0.6, $2/3$, 0.7, 0.8, 0.9, and 1. The result is shown in Figure 3. It is seen that if the block ratio of the solvent-phobic subchain is too short(i.e., if $f_B < 1/3$), the block copolymer acts as the solvent-philic homopolymer. Thus, the system is homogeneous and the micellar structure is not formed. By increasing the block ratio of the solvent-phobic subchain, the spherical micelles and cylindrical micelles are formed (the relation between the morphology of micellar structure and the block ratio is studied by Ohta and Nonomura for the strong segregation limit[25]). By increasing the block ratio further, the vesicles are formed. In this case, the block ratio of the solvent-phobic subchain is large, i.e., the block copolymer is a so-called crew-cut block copolymer. If one increases the block ratio further, the block copolymer acts as the solvent-phobic homopolymer and causes macrophase separation to form droplets.

4.2. AB Diblock Copolymer/A Homopolymer Blends. We now study the AB diblock copolymer/A homopolymer blends. As in the case of solutions, the AB diblock copolymers form micelles in the matrix of A homopolymers.

From the technical viewpoint, simulation of polymer blends is easier than the simulation of polymer solutions because strong segregation is easily achieved in polymer blends for small χ parameters; a large χ parameter makes the interface sharper and causes numerical stability problems at the interface.

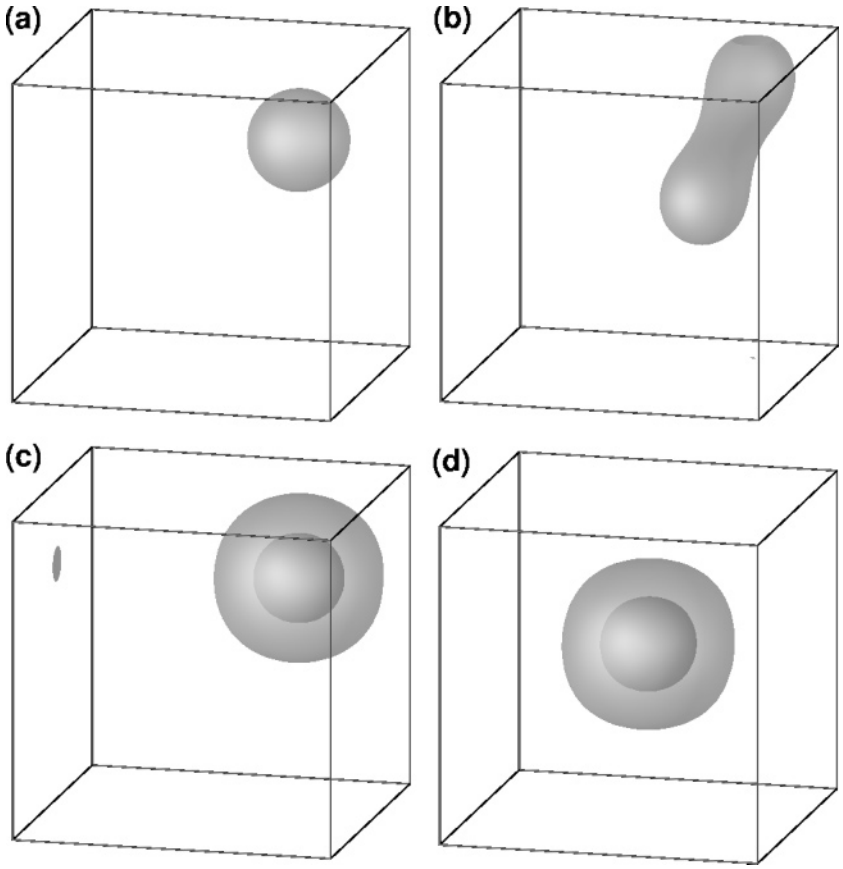

Figure 7. Results of simulations with different χ parameters. The system size is $32b \times 32b \times 32b$. $N_{AB} = 20$, $N_A = 10$, $f_A = 1/3$, $f_B = 2/3$, $\bar{\phi}_{AB} = 0.1$, and $\bar{\phi}_A = 0.9$. (a) $\chi_{AB} = 0.0475$, (b) $\chi_{AB} = 0.525$, (c) $\chi_{AB} = 0.75$, and (d) $\chi_{AB} = 1$. The gray surfaces are isodensity surfaces for $\phi_B(\boldsymbol{r}) = 0.5$.

Figure 4 shows an example of the simulation result for a large system. Here, the system involves $128 \times 128 \times 128$ lattice points (the system size is $64b \times 64b \times 64b$), and the parameters are set to be $N_{AB} = 20$, $N_A = 10$, $f_A = 1/3$, $f_B = 2/3$, $\chi_{AB} = 1$, $\bar{\phi}_{AB} = 0.1$, and $\bar{\phi}_A = 0.9$. In this case, vesicles can be observed more clearly than in Figure 1c. This is considered to be due to the change of the strength of segregation (the segregation of this system is stronger than the system of Figure 1c).

Various self-organized structures can be formed, depending on the parameters such as the block ratio f_A, f_B, the volume fraction $\bar{\phi}_{AB}$ and the χ parameter χ_{AB}. To study the relation between these parameters and the micellar structure, we conducted a simulation of a smaller system that involves $64 \times 64 \times 64$ lattice points. The polymerization index for the AB diblock copolymer and the A homopolymer is set to $N_{AB} = 20$ and $N_A = 10$, respectively.

Morphological change can be observed by chaining the parameters. Figure 5 shows the effect of the block ratio f_A, f_B. Other parameters are set to $\bar{\phi}_{AB} = 0.1$, $\phi_A = 0.9$, and $\chi_{AB} = 1$. If the B block is small (Figure 5a, $f_B = 1/3$), the diblock copolymer forms a spherical micelle that consists of the inner core made of B block and the outer corona made of A block. As the fraction of the B block increases, the spherical micelles become unstable, and vesicles consisting of a bilayer of the block copolymers is formed (Figure 5b, $f_B = 0.5$). The thickness of the B block in the bilayer increases with the increase of the B block ratio. Finally, when f_B becomes equal to unity, the macrophase separation between the A homopolymer and the B homopolymer is observed (Figure 5d, $f_B = 1$). This behavior is just the same as one of the block copolymer solutions. Figure 6 shows the effect of $\bar{\phi}_{AB}$, the volume fraction of diblock copolymers. Other parameters are set to $f_A = 1/3$, $f_B = 2/3$, and $\chi_{AB} = 1$. As the volume fraction of the diblock copolymer increases, the micellar structures change from the spherical micelles to the cylindrical micelles and vesicles. Figure 7 shows the effect of the χ parameter between monomer A and monomer B. Other parameters are set to $f_A = 1/3$, $f_B = 2/3$, $\bar{\phi}_{AB} = 0.1$, and $\bar{\phi}_A = 0.9$. As the χ parameter increases, (i.e., as the antagonicity between the monomers A and B increases), the structures change from the spherical micelles to the cylindrical micelles and then to vesicles. This behavior is just like the case of the volume fraction change.

These results are considered to be consistent with the experimental results of Eisenberg et al.[1,26,27] They studied the morphology of diblock copolymers in a mixed solvent (water plus dioxane) for various block copolymer concentrations and for various solvent compositions and observed the change of the micellar shape from sphere to cylinder and then to vesicles as the water content of the solvent increased. If one regards the change of the water content as the change of the χ parameter between the solvent and the subchain of block copolymer that forms the core, our results are qualitatively in agreement with their experiments.

To demonstrate the similarity between the experimental results and our simulations, we conducted the simulation in the parameter space of $\bar{\phi}_{AB}$ and χ_{AB}. Figure

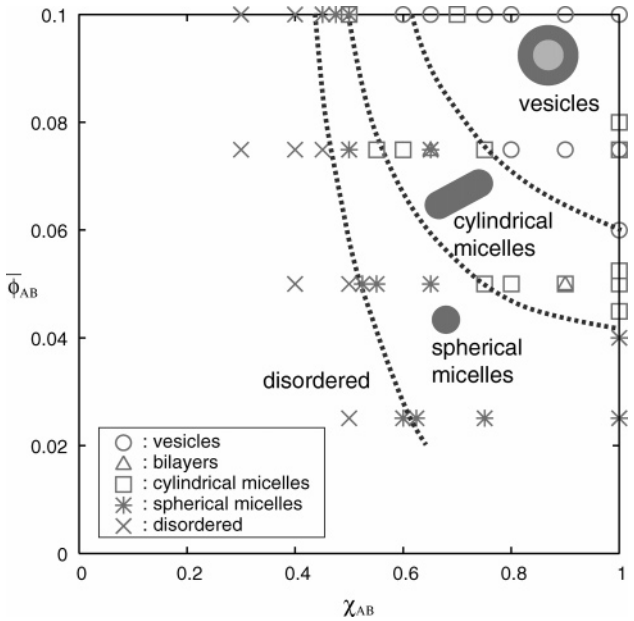

Figure 8. Phase diagram of AB diblock copolymer/A homopolymer blends. The plotted symbols (circles, squares, etc.) correspond to the result of simulations with various χ_{AB} and $\bar{\phi}_{AB}$. The bilayer phase means open, disklike micelles (actually, it is observed experimentally[27]).

8 shows the result. The figure is in qualitative agreement with Figure 6 in ref 26. Note that our simulations were not done for large systems and the size of the simulation cell may affect the final micellar structure (the finite size effect or the effect of the periodic boundary conditions).

5. Discussion

The micellar structures, including vesicles, can be formed for the AB diblock copolymer solutions by using the free-energy model eq 1. The diblock copolymer density is dilute in our systems, and the diblock copolymer is strongly localized at the micellar structures (i.e., the system is the strong segregation). Note that such systems are difficult to treat by the previous density functional approaches. Our free energy model can handle these systems qualitatively correctly, and the simulation with our model is much faster than that of the real-space SCF simulation.

The dynamic vesicle formation process, however, cannot be discussed by our numerical scheme because our scheme does not satisfy the local conservation of mass. This is in contrast to the particle methods (BD[8] and DPD[7]). Nevertheless, it is instructive to study the process of the micellar formation based on our model.

The vesicle formation process for the AB diblock copolymer/A homopolymer blend by our scheme is shown in Figure 9 ($\bar{N}_{AB} = 20$, $N_A = 10$, $f_A = 1/3$, $f_B = 2/3$, $\chi_{AB} = 1$, $\bar{\phi}_{AB} = 0.1$, $\bar{\phi}_A = 0.9$, system size $32b \times 32b \times 32b$, lattice points $64 \times 64 \times 64$, $\omega^{(1)} = 0.5$). It is observed that the nucleus of a micellar structure is first formed by the association of block copolymers (the matrix polymer is expelled from the micellar structure at this stage). The micellar structure then grows, taking solvent into its core from the surroundings, and finally, the vesicle is formed.

This process is the same as that observed by He et al.[20] in their 2D simulation using the SCF method.

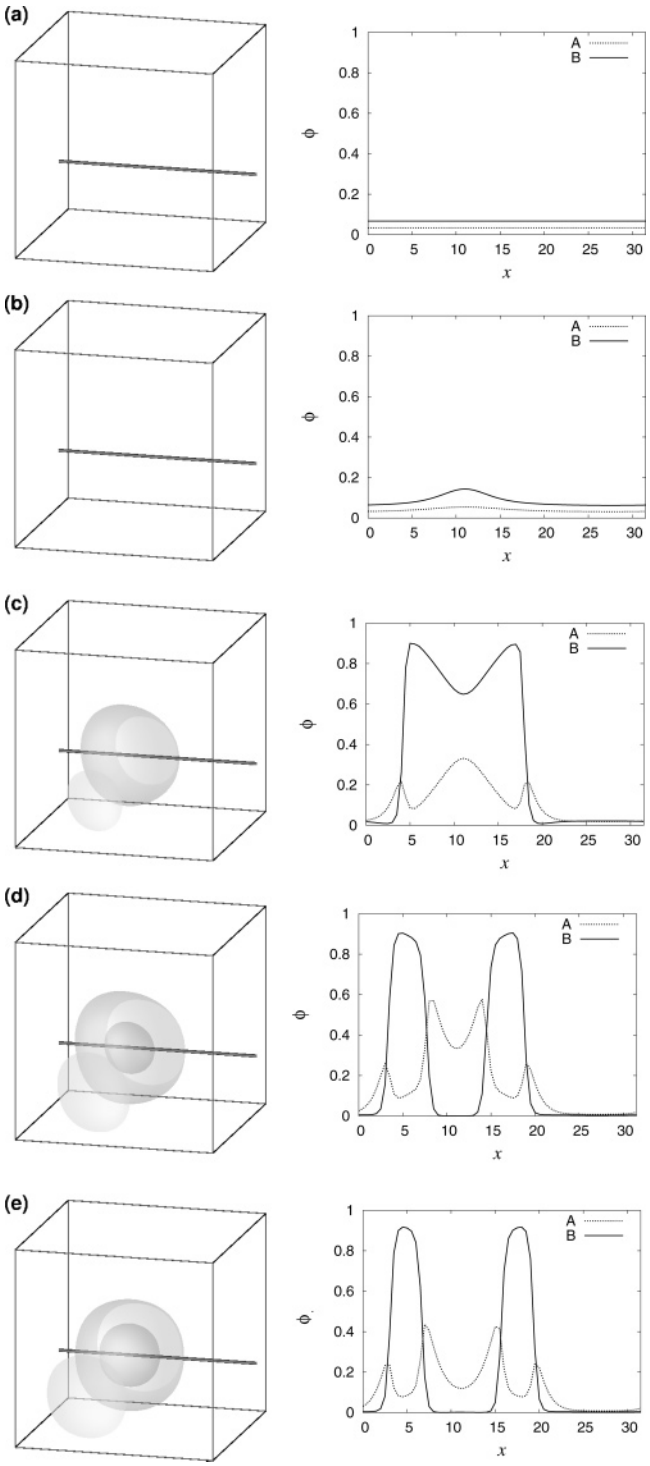

Figure 9. Snapshot of vesicle formation process for the AB diblock copolymer/A homopolymer blend. Number of iteration step = 0, 470, 500, 530, and 990 for (a), (b), (c), (d), and (e), respectively. $\bar{N}_{AB} = 20$, $N_A = 10$, $f_A = 1/3$, $f_B = 2/3$, $\chi_{AB} = 1$, $\bar{\phi}_{AB} = 0.1$, and $\bar{\phi}_A = 0.9$. System size $32b \times 32b \times 32b$, lattice points $64 \times 64 \times 64$. (The parameters are the same as Figure 4 except for the system size.)

(They also used the nonconserving scheme for the evolution of the local density.) According to the scenario of He et al., the nucleus of micellar structures grows first. If the nucleus grows sufficiently large, the nucleus takes solvent into the core because the hydrophilic subchains localized at the large micelles are energetically unfavorable. Finally, the micellar structure changes

their shape from the spherelike structure into a shell-like structure, and thus vesicles are formed.

Therefore, our vesicle formation process is the same as the one of He et al.. This agreement implies that the schemes that do not satisfy the local conservation can form vesicles easily compared with the schemes that are based on the dynamics and satisfy the local conservation (for example, the Cahn−Hilliard type TDGL equation or the dynamic SCF method[13]). The dynamic vesicle formation process based on the continuous field model simulation is for a future work.

6. Conclusion

We have shown that the self-organized structure of block copolymers in solvent can be predicted by the density functional theory using the free energy proposed in ref 23. This is the first 3D simulation of vesicle formation by using the continuous field model. Because the theory can take into account the actual structure of polymers (degree of polymerization, block ratio, topological structure), it will be useful to understand and to predict the micellar structure of surfactant systems.

Appendix

A. Form of Matrixes A_{ij}, C_{ij}. The matrixes A_{ij}, C_{ij} for a diblock copolymer are represented as follows.[23]

$$A_{ij} = \frac{9}{N_{AB}{}^2 b^2 f_A{}^2 f_B{}^2}\begin{bmatrix} f_B^2 & -f_A f_B \\ -f_A f_B & f_A^2 \end{bmatrix} \tag{20}$$

$$C_{ij} = \frac{1}{N_{AB}} \begin{bmatrix} \tilde{S}_{AA}^{-1}\left(\sqrt{\frac{3}{f_A}}\right) - \frac{1}{f_A}\sqrt{\frac{3}{f_A}} & -\frac{1}{4f_A f_B} \\ -\frac{1}{4f_A f_B} & S_{BB}^{-1}\left(\sqrt{\frac{3}{f_B}}\right) - \frac{1}{f_B}\sqrt{\frac{3}{f_B}} \end{bmatrix} \tag{21}$$

where $\tilde{S}^{1-}(\xi)$ is the inverse matrix for the normalized scattering function matrix $\tilde{S}(\xi)$ for the ideal systems.

$$\sum_j \tilde{S}_{ij}(\xi)\tilde{S}_{jk}^{-1}(\xi) = \delta_{ik} \tag{22}$$

$\tilde{S}(\xi)$ is defined as follows.

$$\tilde{S}_{ij}(\xi) = \begin{bmatrix} \frac{2}{\xi^2}(e^{-f_A\xi} - 1 + f_A\xi) & \frac{1}{\xi^2}(e^{-f_A\xi} - 1)(e^{-f_B\xi} - 1) \\ \frac{1}{\xi^2}(e^{-f_A\xi} - 1)(e^{-f_B\xi} - 1) & \frac{2}{\xi^2}(e^{-f_B\xi} - 1 + f_B\xi) \end{bmatrix} \tag{23}$$

B. Chemical Potential. The chemical potential for the system can be calculated by substituting eq 4 into eq 12. The chemical potential for the A,B subchains and S solvent is as follows.

$$\mu_A(\boldsymbol{r}) = \sum_{j(=A,B)} \int d\boldsymbol{r}' 4\sqrt{f_A f_j} A_{Aj} \mathcal{G}(\boldsymbol{r} - \boldsymbol{r}')\psi_j(\boldsymbol{r}') + 2f_A C_{AA}[2\psi_A(\boldsymbol{r}) \ln \psi_A(\boldsymbol{r}) + \psi_A(\boldsymbol{r})] + 4\sqrt{f_A f_B} C_{AB}\psi_B(\boldsymbol{r}) - \frac{b^2}{3}\nabla^2\psi_A(\boldsymbol{r}) + \sum_{j(=A,B,S)} 2\chi_{A,j}\psi_j^2(\boldsymbol{r})\psi_A(\boldsymbol{r}) \tag{24}$$

$$\mu_B(\boldsymbol{r}) = \sum_{j(=A,B)} \int d\boldsymbol{r}' 4\sqrt{f_B f_j} A_{Bj} \mathcal{G}(\boldsymbol{r} - \boldsymbol{r}')\psi_j(\boldsymbol{r}') + 2f_B C_{BB}[2\psi_B(\boldsymbol{r}) \ln \psi_B(\boldsymbol{r}) + \psi_B(\boldsymbol{r})] + 4\sqrt{f_A f_B} C_{AB}\psi_A(\boldsymbol{r}) - \frac{b^2}{3}\nabla^2\psi_B(\boldsymbol{r}) + \sum_{j(=A,B,S)} 2\chi_{B,j}\psi_j^2(\boldsymbol{r})\psi_B(\boldsymbol{r}) \tag{25}$$

$$\mu_S(\boldsymbol{r}) = \frac{2}{N_S}[2\psi_S(\boldsymbol{r}) \ln \psi_S(\boldsymbol{r}) + \psi_S(\boldsymbol{r})] - \frac{b^2}{3}\nabla^2\psi_S(\boldsymbol{r}) + \sum_{j(=A,B,S)} 2\chi_{B,j}\psi_j^2(\boldsymbol{r})\psi_S(\boldsymbol{r}) \tag{26}$$

Note that $\mu_i(\boldsymbol{r})$ contains the Laplacian term $-b^2\nabla^2\psi_i(\boldsymbol{r})/3$ for all i. Thus, the evolution equation, eq 11, can be expressed as

$$\psi_i^{(new)}(\boldsymbol{r}) = \psi_i(\boldsymbol{r}) + \frac{\omega b^2}{3}\nabla^2\psi_i(\boldsymbol{r}) + ... \tag{27}$$

As mentioned before, eq 27 can be solved stably by using an implicit scheme (the ADI scheme, in this work), analogous to the diffusion equation.

References and Notes

(1) Choucair, A.; Eisenberg, A. *Eur. Phys. J.* **2003**, *10*, 37.
(2) Larson, R. G. *J. Chem. Phys.* **1988**, *89*, 1642.
(3) Larson, R. G. *J. Chem. Phys.* **1989**, *91*, 2479.
(4) Larson, R. G. *J. Chem. Phys.* **1992**, *96*, 7904.
(5) Bernardes, A. T. *J. Phys. II* **1996**, *6*, 169.
(6) Groot, R. D.; Warren P. B. *J. Chem. Phys.* **1997**, *107*, 4423.
(7) Yamamoto, S.; Maruyama, Y.; Hyodo, S. *J. Chem. Phys.* **2002**, *116*, 5842.
(8) Noguchi, H.; Takasu, M. *Phys. Rev. E* **2001**, *64*, 041913.
(9) Noguchi, H. *J. Chem. Phys.* **2002**, *117*, 8130.
(10) Maiti, A.; McGrother, S. *J. Chem. Phys.* **2004**, *120*, 1594.
(11) Drolet, F.; Fredrickson, G. H. *Phys. Rev. Lett.* **1999**, *83*, 4381.
(12) Fredrickson, G. H.; Ganesan, V.; Drollet, F. *Macromolecules* **2002**, *35*, 16.
(13) Fraaije, J. G. E. M. *J. Chem. Phys.* **1993**, *99*, 9202.
(14) Kawakatsu, T. *Statistical Physics of Polymers*; Springer-Verlag: Berlin, 2004.
(15) Matsen, M. W.; Schick M. *Phys. Rev. Lett.* **1994**, *72*, 2660.
(16) Matsen, M. W. *Phys. Rev. Lett.* **1995**, *74*, 4225.
(17) van Vlimmeren, B. A. C.; Maurits, N. M.; Zvelindovsky, A. V.; Sevink, G. J. A.; Fraaije, J. G. E. M. *Macromolecules* **1999**, *32*, 646.
(18) Lam, Y.-M., Goldbeck-Wood, G. *Polymer* **2003**, *44*, 3593.
(19) Fraaije, J. G. E. M.; Sevink, G. J. A. *Macromolecules* **2003**, *36*, 7891.
(20) He, X.; Liang, H.; Huang, L.; Pan, C. *J. Phys. Chem. B* **2004**, *108*, 1731.
(21) Kawakatsu, T. *Phys. Rev. E* **1994**, *50*, 2856.
(22) Ohta, T.; Ito, A. *Phys. Rev. E* **1995**, *52*, 5250.
(23) Uneyama, T.; Doi, M. *Macromolecules* **2005**, *38*, 196.
(24) Press, W. H.; Teukolsky, S. A.; Vetterling, S. A.; Flannery, B. P. *Numerical Recipes in C,* 2nd ed.; Cambridge University Press: New York, 1992.
(25) Ohta, T.; Nonomura, M. *Eur. Phys. J. B* **1998**, *2*, 57.
(26) Shen, H.; Eisenberg, A. *J. Phys. Chem. B* **1999**, *103*, 9473.
(27) Shen, H.; Eisenberg, A. *Macromolecules* **2000**, *33*, 2561.

MA0507746